Chemosphere 306 (2022) 135636

Contents lists available at ScienceDirect

Chemosphere

journal homepage: www.elsevier.com/locate/chemosphere

Arsenic(V) immobilization in fly ash and mine tailing-based geopolymers: Performance and mechanism insight

Alseny Bah, Jie Jin, Andrea O. Ramos, Yang Bao, Mengyu Ma, Feihu Li *

Collaborative Innovation Centre of Atmospheric Environment and Equipment Technology, Jiangsu Key Laboratory of Atmospheric Environment Monitoring and Pollution Control, School of Environmental Science and Engineering, Nanjing University of Information Science and Technology (NUIST), 219 Ningliu Road, Nanjing, 210044, China

HIGHLIGHTS

- A low-carbon fly ash/mine tailing-base geopolymer was developed.
- The geopolymers have high mechanical strengths and long-term stabilities.
- It can efficiently immobilize exogenous As^V in addition to the intrinsic As^V.
- Calcite and calcium silicate hydroxide contribute mainly to immobilizing As^V.
- The As^V-immobilized geopolymers can be further used as construction materials.

GRAPHICAL ABSTRACT

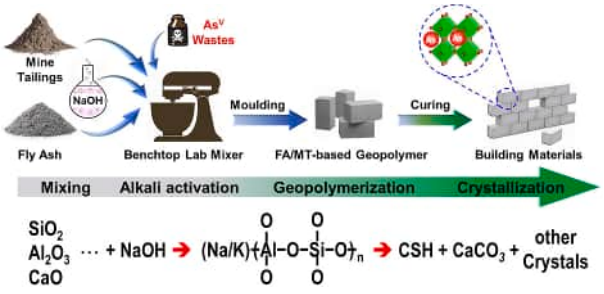

ARTICLE INFO

Handling Editor: Grzegorz Lisak

Keywords:
Geopolymerization
Alkali-activator
Solidification/stabilization
Arsenate
Waste cycling

ABSTRACT

Global mining activities produce thousands of millions of toxic-bearing mine tailing (MT) wastes each year. Storage of the mine tailings not only encroaches upon large areas of cropland but also arouses additional ecological and environmental risks. Herein we demonstrate that geopolymerization of a mixture of the toxic-bearing mine tailings and the coal fly ash (FA) can effectively immobilize exogenous arsenic (As) species in addition to inherent As from the raw materials. The geopolymers also possess high compressive strengths (e.g., >25 MPa for specimens with 54 wt% FA and activated with 10 M sodium hydroxide (NaOH)), allowing them to be further used as low-carbon, cement-free building materials. The geopolymer strength was found to depend clearly upon the NaOH concentration, the FA content, and the curing time, with the maximum being 37.07 MPa for a specimen with 54 wt% FA, 0.03 wt% As, activated with 10 M NaOH and cured for 28 days. Leaching tests showed that all specimens achieved an immobilization efficiency as high as 95.4% toward As, and that both the short-term and long-term leachabilities of all toxic elements are far below the standard maximum contaminant levels. Microstructural analyses indicate that calcite, calcium silicate, and calcium silicate hydroxide are likely to play a crucial role in immobilizing As species and heavy metals of concern in the geopolymer matrixes. Given the superior mechanical strengths and long-term stabilities, the FA/MT-based geopolymers demonstrate a promising low-carbon material for both the remediation of As-bearing lands and the construction industry.

* Corresponding author.
E-mail address: fhli@nuist.edu.cn (F. Li).

https://doi.org/10.1016/j.chemosphere.2022.135636
Received 2 May 2022; Received in revised form 1 July 2022; Accepted 3 July 2022
Available online 7 July 2022
0045-6535/© 2022 Elsevier Ltd. All rights reserved.

1. Introduction

Arsenic (As) contamination in water environments (e.g., mine drainage, groundwater, etc.) and soils due to mining activities have raised the risk of arsenic exposure to crop plants (e.g., rice), animals, and humans, and thus aroused growing concern from across the world (Podgorski and Berg, 2020). China holds approximately 70% of the world's arsenic reservoirs (Li et al., 2016). The mining of lead, zinc, and copper ores produced over 32 million tons of arsenic-bearing mine tailing (MT) wastes annually, predominantly in Hunan province, China (Li et al., 2019). In severe situations, these arsenic residues can contaminate the surrounding soils and groundwater, causing serious threats to the sustainability of agroecosystems and food safety. To address this issue, a variety of technologies, including adsorption, bioremediation, chemical-enhanced washing, chemical precipitation, electrocoagulation, electrokinetic method, ion-exchange, membrane filtration, phytoremediation, solidification/stabilization (S/S), etc. have been widely exploited and well documented in the literature (Alka et al., 2021; Nidheesh and Singh, 2017; Singh et al., 2015). In spite of soil remediation, adsorption, chemical-enhanced washing, precipitation, and phytoremediation are effective in sequestering and/or immobilizing arsenic, however, both the economic and the environmental restrictions limit their application on a large scale (Wang et al., 2019).

Pozzolanic-based solidification/stabilization (S/S) is a well-established, effective, yet cost-efficient remediation technology to immobilize hazardous wastes in contaminated soils and sludges (Palansooriya et al., 2020). Arsenic can be effectively immobilized using ordinary Portland cement (OPC) (Choi et al., 2009; Singh and Pant, 2006) and magnesium phosphate cement (Devi et al., 2020; Wang et al., 2020) as the major cementitious materials. However, the high carbon footprint associated with the production of both types of cement makes the cement-based S/S technology less appealing in the scenario of global carbon neutrality by the middle of the century (Shi et al., 2019). To this end, low-carbon, high-efficiency S/S technologies using massive industrial by-products, e.g., fly ash (FA), red mud, blast-furnace and/or smelting slag, mine tailings (MTs), flue gas desulfurization (FGD) gypsum (Gp), etc. as the alternative cementitious materials have received much attention and also been extensively studied (Jiang et al., 2022; Tian et al., 2021; Wang et al., 2020).

Of various low-carbon S/S technologies, geopolymerization of the mixture of arsenic-bearing waste and the silica- and/or alumina-rich industrial solid wastes (e.g., fly ash, red mud, mine tailing, etc.) by alkali activation has been demonstrated to be an effective alternative to immobilize arsenic into the geopolymer matrix (Diaz-Loya et al., 2012; Tian et al., 2021; Zhou et al., 2021). Geopolymer binders derived from both the alkali activation of coal fly ash (Diaz-Loya et al., 2012) and the high-energy ball milling activation of granulated lead smelting slag (Liu et al., 2019) have shown excellent ability to stabilize the municipal solid waste incinerator fly ash (MSWI FA) with high arsenic content. Recently, it was reported that red mud-metakaolin (MK) based geopolymer shows a good arsenic retention capability as well as a high compressive strength (~15 MPa), making it an environmentally friendly backfilling material for sustainable remediation of arsenic pollution (Zhou et al., 2021). However, the production of MK by calcining kaolinite (at 700 °C) can yield high CO_2 emissions, even though kaolinite clays (>40% kaolinite) are inexpensive and widely accessible (Kavitha et al., 2016). Compared to metakaolin-based geopolymers, fly ash and/or mine tailing-based geopolymers have a lower carbon footprint, making them more desirable for use as building materials and as a matrix for immobilizing toxic wastes (Ahmari and Zhang, 2012; Zhang et al., 2011; Zhang, N. et al., 2021). For instance, when using sugar mill lime sludge as a Ca-based activator, it was suggested that coal fly ash and mine tailing-based geopolymer can effectively stabilize the mine tailings with high levels of arsenic and heavy metals. Besides, since the geopolymer has high compressive strength (>7.5 MPa), it can also be used as construction materials (Opiso et al., 2021).

While many studies have demonstrated that geopolymer matrix plays a crucial role in the immobilization of arsenic wastes, the underlying mechanisms remain poorly understood due to the contradictory results that have often been presented. During the geopolymerization process, arsenic can react either with calcium-rich components to form calcium arsenate precipitates, with Friedel's salt to yield As-Friedel's salt mineral, or with the geopolymer gels (e.g., calcium (alumino)silicate hydrate) to form surface complexes (Jiang et al., 2022; Liu et al., 2019). Zhou et al. claimed that ion exchange with ettringite, formation of Ca–As and Fe–As precipitates, and physical encapsulation with geopolymer gel were the predominant mechanisms for stabilizing arsenic (Zhou et al., 2021). However, other studies showed that arsenic exhibits a poor immobilization potential in geopolymer systems due to its high pH sensitivity (Giels et al., 2019; Izquierdo et al., 2009). In this regard, the interactions between arsenic and the mine tailing-based geopolymer matrix and the immobilization mechanism of arsenic should be further elucidated.

In this study, we focus on the feasibility of immobilizing exogenetic arsenate (As^V) in geopolymer matrices derived from the mixtures of fly ash, lead-zinc mine tailing, and FGD gypsum that were activated with sodium hydroxide and sodium silicate solution. The geopolymer specimens were investigated at different As^V contents, NaOH concentrations, fly ash contents, curing time, etc. to explore the mechanic properties, microstructure, As^V leaching characteristics, and the immobilization mechanism of arsenic by using unconfined compressive strength (UCS) test, X-ray diffraction (XRD), scanning electron microscopy (SEM), Fourier Transform Infrared (FTIR), and X-ray photoelectron spectroscopy (XPS) analyses.

2. Materials and methods

2.1. Materials

The raw materials used in this study include lead-zinc (Pb–Zn) mine tailings (MTs), class F fly ash (FA), and FGD gypsum (Gp). Both the FA and the Gp were obtained from Jiangsu Nanre Power Generation Co., Ltd. (Nanjing, China). The MT was provided by Nanjing Yinmao Pb–Zn Mining Industry Co., Ltd. (Nanjing, China). The mineral constituents, chemical compositions and trace heavy metals of both the FA and the MT can be found elsewhere (Bah et al., 2022). The FDG gypsum consists of kidney bean-shaped powders of size ranging from ~10 to ~55 μm, with almost pure gypsum ($CaSO_4{\cdot}2H_2O$, JCPDS #33–0311) as well as trace metals (see Fig. S1in the Supplementary data).

Reagent grade 96% NaOH pellets were purchased from Macklin Biochemical Co., Ltd. (Shanghai, China). Sodium silicate (SS) solution with silica to sodium oxide molar ratio of 2:2–2:2.31 was obtained from Ganjiashan Yourui Refractories Co., Ltd. (Nanjing, China). Sodium arsenate dibasic heptahydrate ($Na_2HAsO_4{\cdot}7H_2O$, 98%) was purchased from Sigma-Aldrich (Shanghai, China) and used as the arsenate source. All chemicals were used as received without further purification. Deionized water was used in preparation solutions and the geopolymer.

2.2. Preparation of geopolymer

For the preparation of FA/MT-based geopolymer, FA was fully mixed with MT by using a benchtop laboratory mixer (NJ-160A, Wuxi Jianyi I&M Co., Ltd, China) at a given content, i.e., 28 wt%, 44 wt%, 54 wt%, and 61 wt% (by total solid mass) to form a dry-blend. Then the NaOH (5, 8, and 10 M) together with 25 g of SS and deionized water were slowly added to the above dry-blend while mixing gently until a homogeneous paste was formed. The liquid to solid (L/S) ratio was kept at 0.33–0.34 to achieve a paste with good workability. The resultant paste was then cast into the six-fold concrete cube test steel moulds ($20 \times 20 \times 20$ mm^3) at room temperature for 24 h. The shaped cubic geopolymer specimens were demoulded carefully and then placed in a blast drying oven for barely curing at 65 °C for another 24 h. After cooling, the specimens

Table 1
Geopolymer specimen composition matrix and characterization tests conducted.

Specimen ID	NaOH (M)	FA content (wt.%)	Gp content (wt.%)	As^V content (wt.%)	Si/Al [a]	Na/Al [a]	Curing time (days)	UCS test	XRD	SEM	FTIR
FMA5G-02a	5	54	2.5	0.01	0.83	0.41	7, 14, 28	X [b]		X	
FMA5G-02b	5	54	2.5	0.03	0.83	0.41	7, 14, 28	X	X	X	X
FMA5G-02c	5	54	2.5	0.05	0.83	0.41	7, 14, 28	X		X	
FMA8G-02a	8	54	2.5	0.01	0.83	0.52	7, 14, 28	X			
FMA8G-02b	8	54	2.5	0.03	0.83	0.52	7, 14, 28	X		X	
FMA8G-02c	8	54	2.5	0.05	0.83	0.52	7, 14, 28	X	X	X	X
FMA10G-01a	10	61	2.5	0.01	0.94	0.46	7, 14, 28	X	X	X	
FMA10G-01b	10	61	2.5	0.03	0.94	0.46	7, 14, 28	X			
FMA10G-01c	10	61	2.5	0.05	0.94	0.46	7, 14, 28	X		X	
FMA10G-02a	10	54	2.5	0.01	0.83	0.60	7, 14, 28	X	X	X	X
FMA10G-02b	10	54	2.5	0.03	0.83	0.60	7, 14, 28	X	X	X	X
FMA10G-02c	10	54	2.5	0.05	0.83	0.60	7, 14, 28	X	X	X	X
FMA10G-03a	10	44	2.5	0.01	0.68	0.87	7, 14, 28	X		X	
FMA10G-03b	10	44	2.5	0.03	0.68	0.87	7, 14, 28	X			
FMA10G-03c	10	44	2.5	0.05	0.68	0.87	7, 14, 28	X		X	
FMA10G-04a	10	28	2.5	0.01	0.43	1.62	7, 14, 28	X		X	
FMA10G-04b	10	28	2.5	0.03	0.43	1.62	7, 14, 28	X			
FMA10G-04c	10	28	2.5	0.05	0.43	1.62	7, 14, 28	X			
FMA5G5-02a	5	54	5	0.01	0.83	0.41	7, 14, 28	X			
FMA5G5-02b	5	54	5	0.03	0.83	0.41	7, 14, 28	X			
FMA5G5-02c	5	54	5	0.05	0.83	0.41	7, 14, 28	X			
FMA8G5-02a	8	54	5	0.01	0.83	0.52	7, 14, 28	X	X	X	X
FMA8G5-02b	8	54	5	0.03	0.83	0.52	7, 14, 28	X		X	
FMA8G5-02c	8	54	5	0.05	0.83	0.52	7, 14, 28	X			
FMA10G5-02a	10	54	5	0.01	0.83	0.60	7, 14, 28	X	X	X	X
FMA10G5-02b	10	54	5	0.03	0.83	0.60	7, 14, 28	X			
FMA10G5-02c	10	54	5	0.05	0.83	0.60	7, 14, 28	X		X	

[a] Note: the calculated Si/Al and Na/Al ratios in the initial mixtures are not necessarily the same as the final ratios in the geopolymer gels.
[b] X indicates test has been conducted.

were left in the lab tray with a PE film covering and cured at room temperature for 7, 14, and 28 days before further tests. All geopolymer specimens were prepared in triplicate. To study the effect of Gp content on the mechanical strength as well as the As^V immobilization performance of the FA/MT-based geopolymer specimens, 2.5 wt% and 5 wt% of Gp (by total solid mass) were added into the dry-blend. In the case of preparing geopolymer for As^V immobilization, 0.01 wt%, 0.03 wt%, and 0.05 wt% of arsenic (by the mass of elemental As) were added along with the NaOH solution. The geopolymer specimen composition matrix is summarized in Table 1.

2.3. Characterization of geopolymer

The unconfined compressive strength (UCS) tests were performed to evaluate the effects of NaOH concentration, incorporated Gp, curing time, and introduction of As^V on the mechanical strength of the resultant geopolymer specimens. After 7-, 14-, and 28-day curing, the geopolymer specimens were tested on a WDW-100 universal material testing machine (Jinan Fangyuan Test Instrument Co., Ltd., China) at a constant loading of 5 MPa/s in terms of the ASTM C109M − 2008 standard. Each geopolymer specimen was tested in triplicate and the average UCS value was used for further analysis.

To investigate the microscopic characteristics of geopolymer, the crushed specimens from the UCS tests were collected and further milled into fine powders for further tests. X-ray diffraction (XRD) analysis was conducted on an XRD-6100 diffractometer (Shimadzu, Japan) at a tube voltage of 40 kV and a tube current of 30 mA with Cu-Kα radiation (step size: 0.02°, scanning rate: 5° min^{-1}). The morphological images of the geopolymer specimens were obtained on a SU1510 (Hitachi, Japan) scanning electron microscope (SEM) at an accelerating voltage of 1.5 kV. Fourier Transform Infrared Spectroscopy (FTIR) data were collected on an Is5 infrared spectrometer (Thermo Nicolet, USA) by using the KBr pellet method. X-ray photoelectron spectroscopy (XPS) analysis was performed on a PHI 5000 spectroscope (Versa Probe, UIVAC-PHI, Japan) equipped with a monochromatized Al Kα X-ray source ($h\nu$ = 1486.6 eV). The C1s peak (284.8 eV) was used for the calibration of binding energy values.

2.4. Leaching tests

To evaluate the leachability of As^V as well as some heavy metals of concern from the FA/MT-geopolymer specimens, all the specimens were crushed into granules with size far less than 9.5 mm and then the Toxicity Characteristic Leaching Procedure (TCLP) tests were conducted following the US EPA test method 1311 (U.S. Environmental Protection Agency, 1992). The leachates were filtered with 0.45 μm filters (Tianjin Navigator Lab Instrument Co., Ltd, China) and acidified with ultrapure nitric acid (Sinopharm Chemical, Shanghai, China) before further analyses. As^V concentrations in the leachates were measured using an Optima™ 8000 Inductively Coupled Plasma-Optical Emission Spectrometry (ICP-OES) analyzer (PerkinElmer Inc., USA). All TCLP tests were performed in triplicate and average values were used. The As^V immobilization efficiency was determined using the following equation,

$$Immobilization\% = \frac{C_0 - C_f}{C_0} \times 100\%$$

where $\mathbf{C}_0$ is the As^V concentration in the initial suspension of the TCLP test by assuming that all As^V in the geopolymer specimens are leachable, while $\mathbf{C}_f$ is the measured As^V concentration in the corresponding leachate ($mg{\cdot}L^{-1}$).

3. Results and discussions

3.1. Effect of NaOH concentration on UCS of the FA/MT-based geopolymers

To investigate the effect of NaOH concentration on the UCS of the FA/MT-based geopolymers, UCS tests were performed on geopolymer specimens with different FA and As^V contents that were activated with 5,

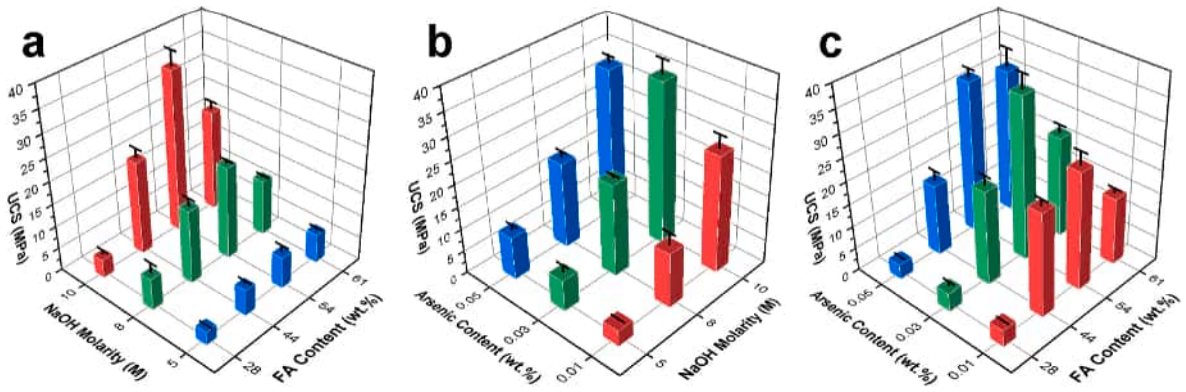

Fig. 1. (**a**) Effect of NaOH concentration and FA content on the 7-day UCS of FT/MT-based geopolymer specimens with a constant As^V content of 0.03 wt%, (**b**) Effect of NaOH concentration and As^V content on the 7-day UCS of specimens with a constant FA content of 54 wt%, (**c**) Effect of As^V and FA contents on the 7-day UCS of specimens activated with 10 M NaOH.

8, and 10 M NaOH, respectively (Fig. 1a and b, S2 and S3). As in the case in Fig. 1a, apart from geopolymers with 28 wt% of FA, the UCS values after curing for 7 days (abbreviated as 7-day UCS) of the FA/MT-based geopolymers increase almost linearly with increasing NaOH concentrations ranging from 5 to 10 M. This near-linear dependency between the UCS and the NaOH concentration is also evident for these geopolymer specimens cured for 14, and 28 days, respectively (Figs. S2 and S3). It is well established that NaOH accelerates the dissolution of silicates and aluminosilicates in aqueous systems (Rees et al., 2007). With increasing NaOH concentrations, UCS is likely to increase because more Na^+ and OH^- react with the silica- and alumina-rich phase, dissolving more Si and Al and thereby increasing the concentration of Si and Al in the liquid phase (Ahmari et al., 2012). Faster dissolution of the aluminosilicate phases may lead to faster geopolymer formation due to rapid conversion of the raw materials. Besides, it is believed that during the formation of geopolymer, Na^+ and OH^- ions also play significant roles in stabilizing aqueous species and colloids, increasing the solubility limits of silica and alumina, reducing electrostatic repulsion between the dissolved anions, and catalyzing geopolymer gel formation and rearrangement (Rees et al., 2007). These will in turn lead to faster geopolymer formation, and thus increase the geopolymer compressive strength. The UCS improvement with NaOH concentration has also been observed previously (Ahmari et al., 2012; Li et al., 2012; Rees et al., 2007), particularly in mixtures with a large number of amorphous aluminosilicate phases (Ahmari et al., 2012; Allahverdi and Kani, 2009). This observation is also validated in the present study that the activation of the FA/MT mixtures with 10 M NaOH resulted in the highest UCS (i.e., 35.52 and 37.07 MPa for 7-day and 28-day UCS, respectively) when the mixture with FA content as high as 54 wt% was used (Fig. 1a and S2b). This is because FA particles contain more amorphous phases than the MT powder and are thereby more reactive to the NaOH solution (Bah et al., 2022).

It is of interest to note, however, that the UCS value of geopolymer specimen activated with 10 M NaOH is lower than that activated with 8 M NaOH in the case of geopolymers with 28 wt% of FA (Fig. 1a and S2). This can be explained by the negative effect of excess NaOH on geopolymer formation which has also been observed previously (Rees et al., 2007; Rowles and O'Connor, 2003). Geopolymer compressive strength is believed to increase with increasing Na/Al molar ratios up to a specific maximum value, above which the strength is reduced (Rees et al., 2007; Rowles and O'Connor, 2003). Based on this argument, it would appear that the Na/Al molar ratio has reached up to the maximum value favorable for the geopolymer formation in the specimen with 28 wt% of FA that was activated with 8 M NaOH.

3.2. *Effect of FA, As^V and Gp contents on UCS*

As shown in Fig. 1a and S2, all UCS values (i.e., 7-, 14- and 28-day UCS) increase with FA contents ranging from 28 wt% to 54 wt%, while decrease to some extent when the FA contents are as high as 61 wt % at NaOH concentrations of 5, 8 and 10 M, respectively. As discussed above, it appears that the Na/Al molar ratios have achieved the optimum value favoring geopolymer formation when the FA contents increased up to 54 wt%, indicating that the FA/MT mixture containing 54 wt% FA is the optimal recipe for geopolymer formation regarding the compressive strength. Further increasing the FA proportion in the FA/MT mixtures will no doubt result in decreased Na/Al molar ratios, and thus declined compressive strengths. This behaviour is in good consistency with the calculated Na/Al data (Table 1) and has also been reported elsewhere (Shan et al., 2012).

In general, Na^+ ions from the alkali activator (e.g., NaOH) can reduce the electrostatic repulsion between the dissolved anions through the formation of ion-pairing complexes (e.g., Si/Al–$O^- \cdots Na^+$), by which to accelerate the geopolymer gel formation (Rees et al., 2007). As mentioned above, 0.01–0.05 wt% of As^V was added to the geopolymer mixtures in the form of sodium arsenate to evaluate the immobilization performance in this study. For instance, the addition of 0.05 wt% of As^V will also introduce 306.5 mg g^{-1} of Na^+ into the geopolymer system. This suggests that the Na^+ ions from sodium arsenate will somewhat contribute to the geopolymer gel formation, particularly when the Na^+ ions from NaOH are very limited. The effect of As^V content on the UCS is distinct in the cases of geopolymer specimens with 54 wt% of FA and 5 M NaOH, which demonstrates that the UCS values increase proportionally as the As^V contents increase from 0.01 wt% to 0.05 wt% (Fig. 1b and S3), confirming the profound contribution from the Na^+ ions of sodium arsenate. Similar observations are also notable in geopolymer specimens with 61 wt% FA and 10 M NaOH as shown in Fig. 1c and S4, where Na^+ ions from NaOH are inadequate to dissolve the amorphous phases in FA of the mixtures, and therefore the introduction of extra Na^+ ions along with As^V sources can result in obvious increases in the compressive strengths. In other geopolymer specimens rich in Na^+ ions from NaOH (with high Na/Al molar ratios) as shown in Fig. 1b and c, S3, and S4, the effect of As^V content appears to be stochastic since excess Na^+ ions in the geopolymer system can reduce the compressive strength (Rees et al., 2007; Rowles and O'Connor, 2003).

Gypsum is known to accelerate the induration and the early strength of the geopolymer, promoting arsenic solidification to some extent (Li et al., 2016; Zhang et al., 2019). Nevertheless, excess gypsum in geopolymer mixture appears to increase the mobility of arsenic (Li et al., 2016; Tigue et al., 2018), and reduce the UCS values of the resultant geopolymer. Considering the leachability of toxics and the compressive strength, adding 8–12 wt% of gypsum to the geopolymer mixture is well

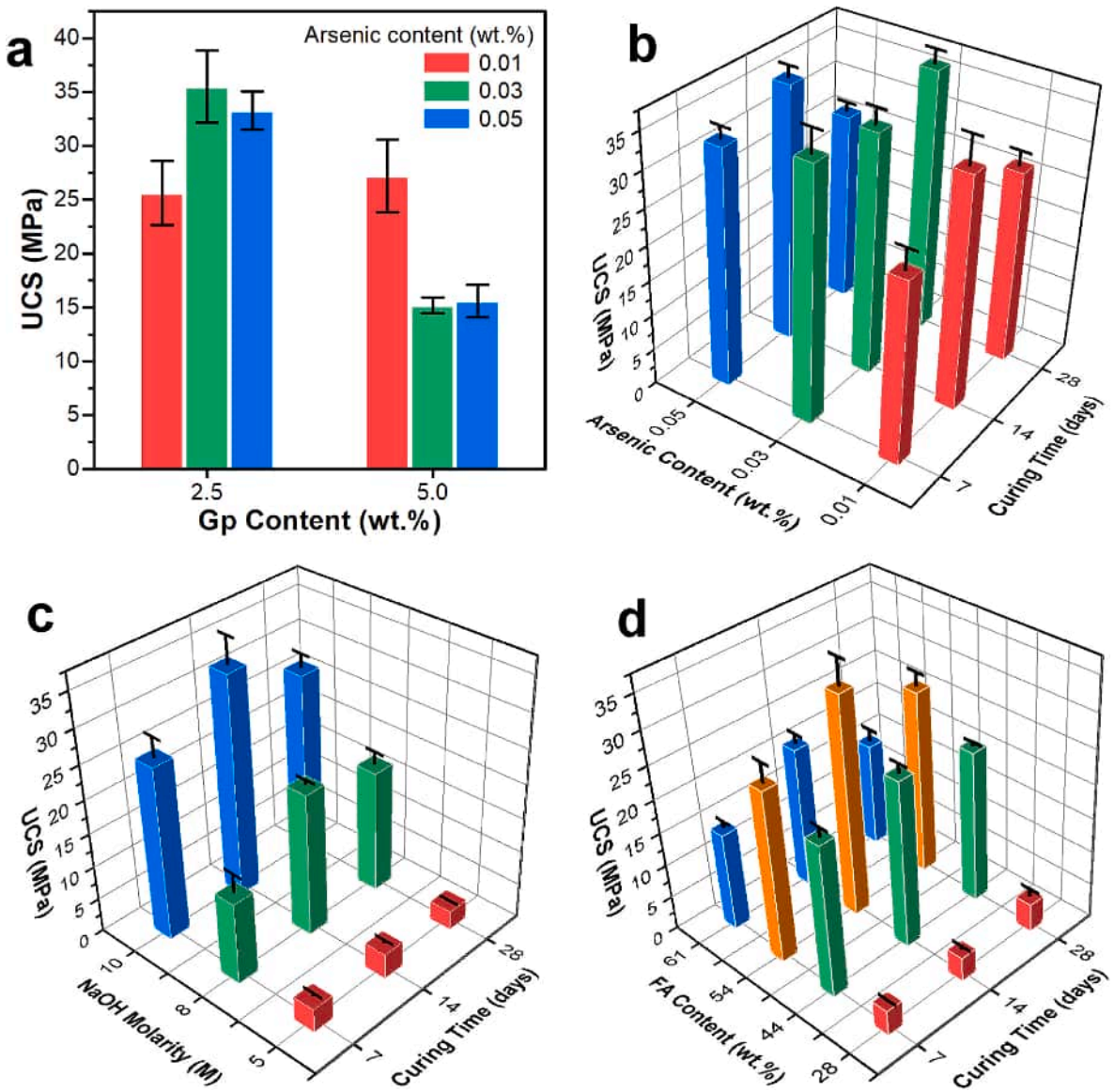

Fig. 2. (**a**) Effect of Gp content on the 7-day UCS of specimens (54 wt% FA, 10 M NaOH); (**b**) Effect of curing time and As^V content on the UCS of the same specimens; (**c**) Effect of curing time and NaOH concentration on the UCS of specimens (54 wt% FA, and 0.01 wt% As^V); and (**d**) Effect of curing time and FA content on the UCS of specimens (0.01 wt% As^V, and 10 M NaOH).

established (Li et al., 2016; Zhang et al., 2019). However, our results in Fig. 2a demonstrate that introduction of 5 wt% of Gp can lead to significant decreases in the UCS values of geopolymers (NaOH = 10 M, FA content = 54 wt%), as compared to those with 2.5 wt% gypsums. Therefore, we mainly focus on the geopolymer mixtures with a Gp content of 2.5 wt% in the present study, and all geopolymer mixtures were blended with 2.5 wt% of Gp unless otherwise specified. Moreover, it is worthy to note that the highest UCS of 39.46 MPa can be found in geopolymer specimens with 61 wt% FA, 0.05 wt% As^V and 10 M NaOH after curing for 14 days (see the supplementary UCS data). Besides, this geopolymer has a 28-day UCS as high as 31.88 MPa. In comparison to conventional FA-based geopolymers (Ahmari et al., 2012; Jiang et al., 2022; Tian et al., 2021), the geopolymer exhibits superior compressive strength, making it an attractive material for use in construction (Capasso et al., 2019; Zhang, X.L. et al., 2021).

3.3. Effect of curing time on UCS

It has been reported previously that for FA-based geopolymer systems the temperature at which specimens are cured significantly affects its final compressive strength (van Jaarsveld et al., 2002). Our previous work has also confirmed that curing at 65 °C can improve the overall strength of the geopolymer specimens as compared to those cured at 25 °C (Bah et al., 2022). Therefore, the effect of curing time on UCS in this study was investigated by evaluating the compressive strength of specimens cured at 65 °C for different curing times. Geopolymer specimens prepared with varying FA and As^V contents, NaOH concentrations, and cured for 7, 14, and 28 days were evaluated and the results are presented in Fig. 2b–d. For all specimens, it appears that the strength of the geopolymers developed rapidly in the first 7 days, accounting for >70% of the maximum UCS values that were obtained in 14 days. This observation is in good agreement with previous reports (Bah et al., 2022; Zhang et al., 2011).

However, it is of interest to note that the 28-day UCS values decreased slightly (i.e., 9.2–16.6%) as compared to the 14-day UCS for most specimens studied (Fig. 2b–d). This may attribute to the inadequate geopolymerization of the mixture due to the initial loss of water during the heating process in an oven at 65 °C (van Jaarsveld et al.,

Table 2
As^V leaching test results (in mg L^{-1}) of geopolymer specimens with different curing time.

Specimen ID	As^V leachability			Specimen ID	As^V leachability			Specimen ID	As^V leachability		
	7 days	14 days	28 days		7 days	14 days	28 days		7 days	14 days	28 days
FMA5G-02a	0.27	0.75	n.d.	FMA10G-02a	0.31	0.02	0.01	FMA5G5-02a	0.48	0.18	n.a.
FMA5G-02b	2.17	1.11	0.84	FMA10G-02b	1.33	0.61	0.01	FMA5G5-02b	0.94	1.42	1.00
FMA5G-02c	2.17	1.96	2.09	FMA10G-02c	2.16	1.87	1.37	FMA5G5-02c	n.d.	2.56	0.87
FMA8G-02a	0.34	1.32	n.d.	FMA10G-03a	0.12	n.d.	0.65	FMA8G5-02a	0.83	n.d.	n.d.
FMA8G-02b	0.58	0.72	0.22	FMA10G-03b	n. d.	0.95	0.09	FMA8G5-02b	1.05	1.33	n.d.
FMA8G-02c	0.82	n. d.	0.83	FMA10G-03c	2.53	1.87	0.78	FMA8G5-02c	2.60	n.d.	1.77
FMA10G-01a	0.08	0.44	0.06	FMA10G-04a	0.70	n. d.	0.41	FMA10G5-02a	0.08	1.05	n.a.
FMA10G-01b	0.57	0.63	0.31	FMA10G-04b	n. d.	0.59	0.07	FMA10G5-02b	1.05	0.81	0.13
FMA10G-01c	0.89	1.20	n.a.	FMA10G-04c	0.94	1.19	0.20	FMA10G5-02c	1.16	0.99	1.44
Chinese standard	**5.0**	**5.0**	**5.0**								

*n.d. = not detected; n.a. = not available.

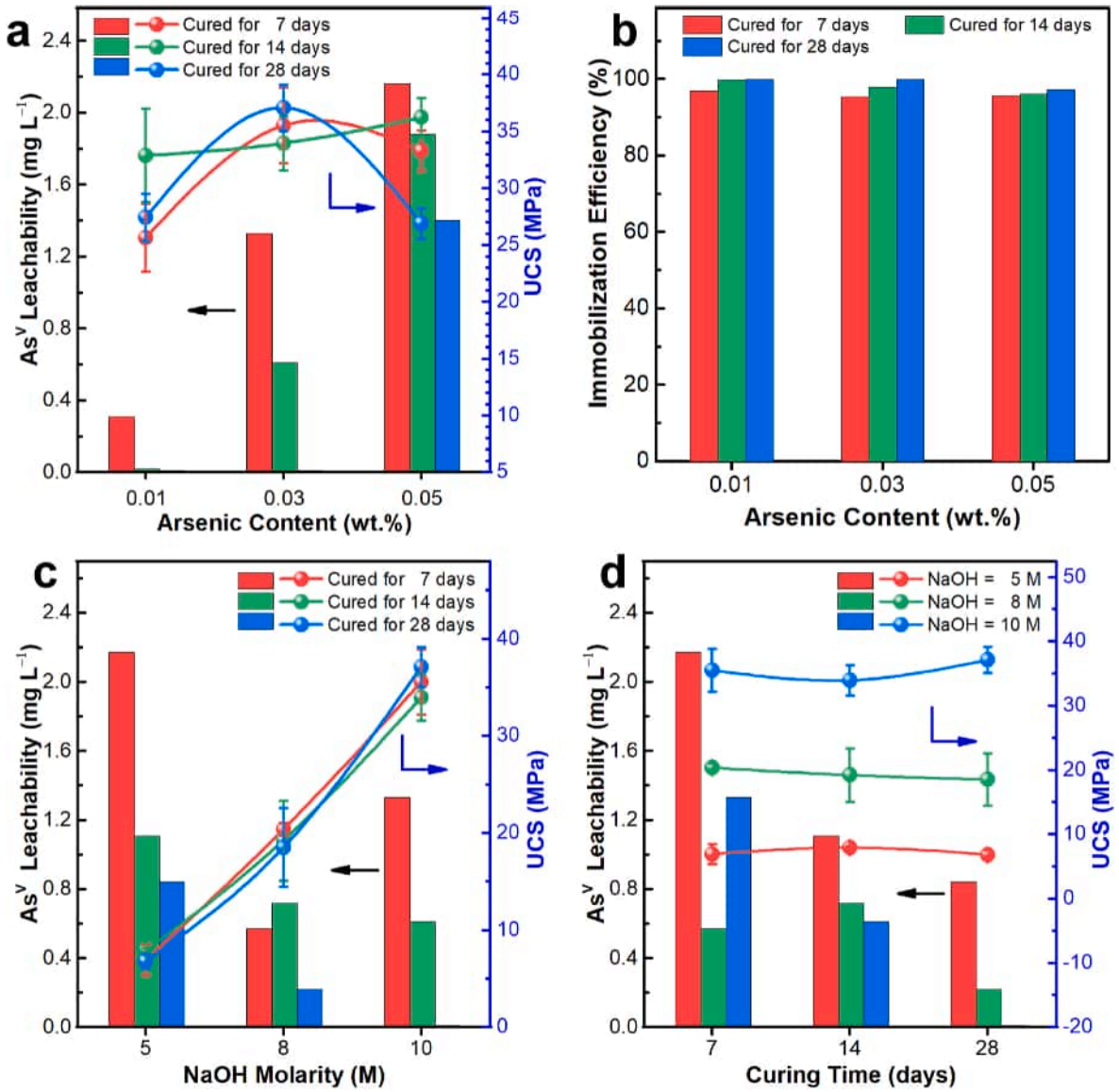

Fig. 3. Effect of As^V content on (**a**) the As^V leachability and the 7-day UCS, and (**b**) the As^V immobilization efficiency of geopolymer specimens (54 wt% FA, 10 M NaOH), (**c**) Effect of NaOH concentration on the As^V leachability and the UCS of specimens cured for 7, 14, and 28 days (54 wt% FA, and 0.03 wt% As^V), (**d**) Effect of curing time on the As^V leachability and the UCS of specimens with 5, 8, and 10 M NaOH (54 wt% FA, and 0.03 wt% As^V).

2002; Zhang, N. et al., 2021), and the reduction in compactness owing to the phase transitions from amorphous gels to crystalline minerals (Devi et al., 2020; Tian et al., 2021). The phase transitions are also confirmed by the XRD data to be discussed later in the following section. Nevertheless, it is apparent that when the specimen was prepared with 54 wt% FA and 10 M NaOH, curing at 65 °C for 24 h can endow the specimen

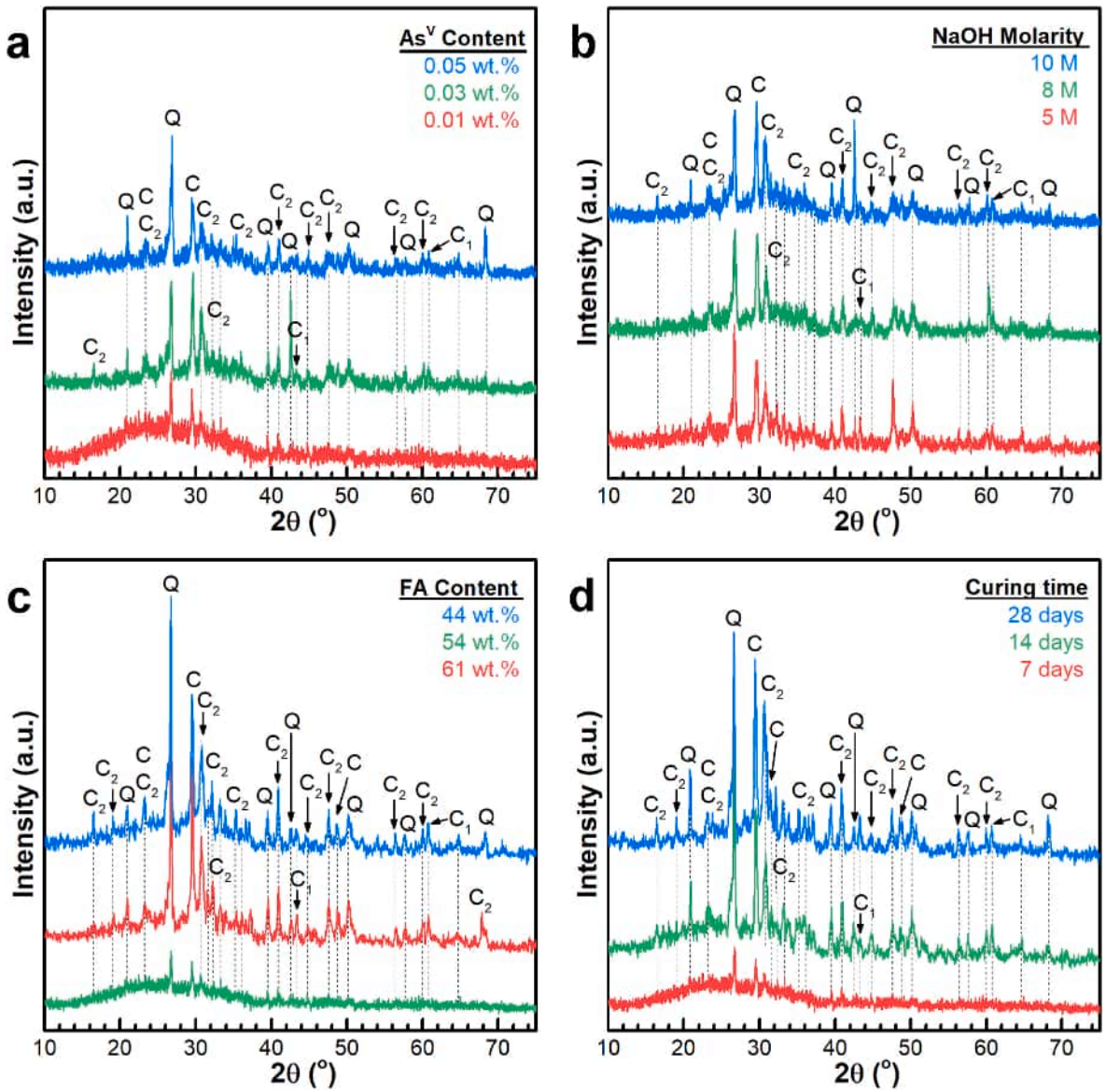

Fig. 4. XRD patterns of (**a**) geopolymer specimens of 54 wt% FA, 10 M NaOH and cured for 7 days with varying arsenic contents; (**b**) specimens of 54 wt% FA, 0.03 wt% As^V, cured for 7 days and activated with 5, 8, and 10 M NaOH; (**c**) specimens of 0.01 wt% As^V, 10 M NaOH and cured for 7 days with varying FA contents; (**d**) specimens of 54 wt% FA, 0.01 wt% As^V, 10 M NaOH, and cured for different days. (**C**: Ca_2SiO_4; **C_1**: $CaCO_3$; **C_2**: $Ca_5(SiO_4)_2(OH)_2$; **Q**: quartz).

with a 7-day UCS as high as 35.52 MPa (Fig. 2b), implying that curing at elevated temperature can not only enhance the early strength of the specimen but also shorten the curing time (Rovnanik, 2010).

3.4. Leaching results of As^V

For geopolymer formation, a compacted and consolidated material with relatively high strength is usually preferable, while low permeability is desirable from a long-term environmental safety perspective when using such geopolymer for the solidification/stabilization of toxic wastes. The TCLP leaching results of As^V as well as typical heavy metals of concern (e.g., Cu, Pb, Cr, etc.) from the raw materials and geopolymer specimen without addition of any exogenous As^V are shown in Table S1. It is obvious that As^V is completely undetectable in both raw materials and the synthetic geopolymer, although earlier XRF results have confirmed the presence of 21.3 and 151.9 ppm As^V in FA and MT, respectively (Bah et al., 2022). In addition, it is interesting to note that only the leachability of Pb (i.e., 16.25 ppm) among the heavy metals of concern in MT exceeded the maximum contaminant level (MCL) by 3.3 times, whereas the leachability of Pb in the synthetic geopolymer was only 0.27 ppm, which is far below the MCL (i.e., 5 ppm). The leachabilities of exogenous As^V from the geopolymer specimens with different compositions and curing times are given in Table 2 and depicted in Fig. 3. The results are quite variable, with leached As^V concentrations in the leachates (i.e., the As^V leachabilities) ranging from 0 (not detected, n.d.) to 2.6 mg L^{-1} (Table 2). In the case of geopolymer specimens with 54 wt% of FA and 10 M of NaOH, curing in the air for 7 days endowed the specimen of 0.03 wt% As^V with the maximum strength (i.e., 35.52 MPa), while presented the highest As^V leachability (i.e., 2.16 mg L^{-1}) to the specimen with 0.05 wt% As^V (Fig. 3a). However, when prolonging the curing time to 14 days, it is of interest to note that both the UCS values and the As^V leachabilities increase proportionally with the As^V contents from 0.01 to 0.05 wt%, which has also been observed previously (Akhter et al., 1997). Further extending the curing time to 28 days resulted in the maximum compressive strength of the specimen with 0.03 wt% As^V (i.e., 37.07 MPa), while the highest As^V leachability of that incorporating 0.05 wt% of As^V (i.e., 1.4 mg L^{-1}). Nevertheless, this is lower than the standard MCL value, confirming its environmental

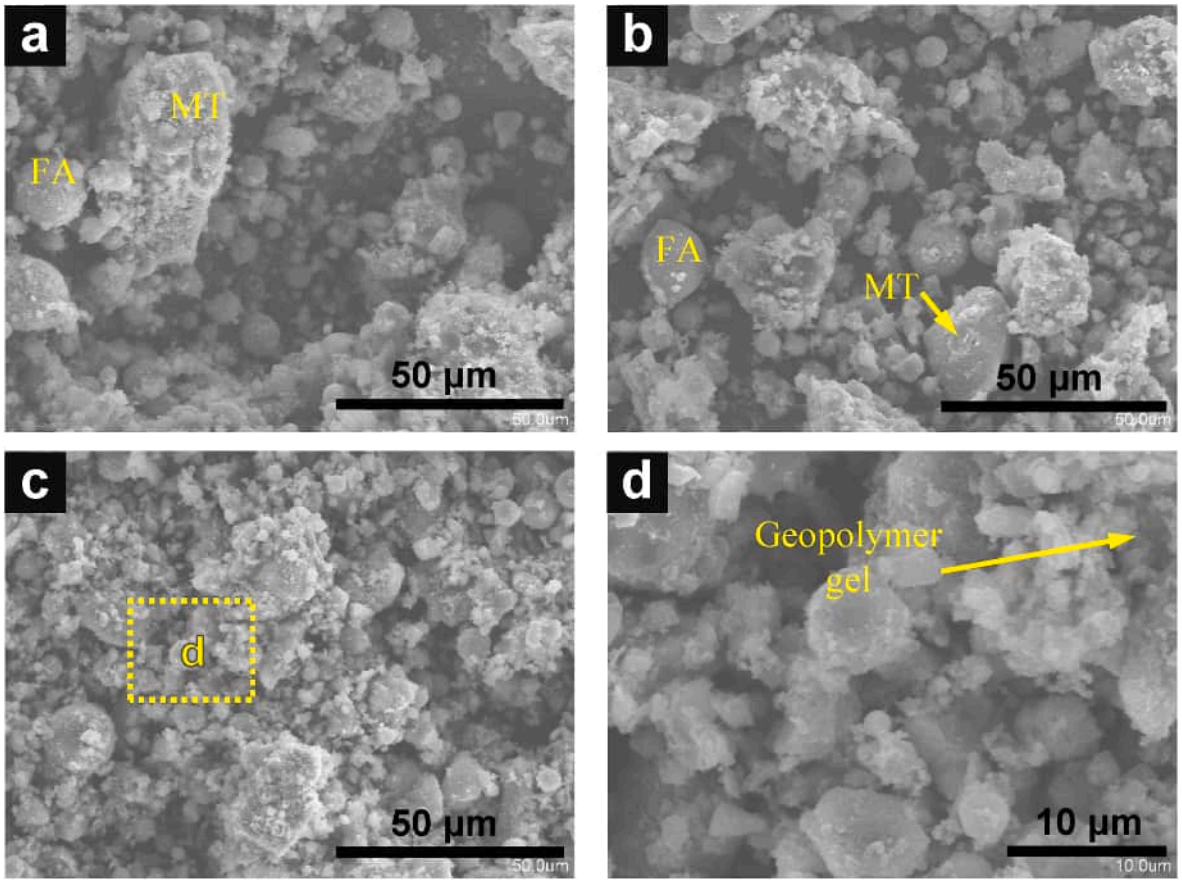

Fig. 5. SEM images of geopolymer specimens of 54 wt% FA, cured for 7 days and activated with (**a**) 5 M NaOH, (**b**) 8 M NaOH, and (**c**, **d**) 10 M NaOH.

benignity.

Results in Fig. 3c indicate that the As^V leachability decreases with increasing NaOH concentrations from 5 to 10 M for specimens with 54 wt% of FA, 0.03 wt% As^V and cured for 14, and 28 days, respectively, whereas the UCS values increase proportionally with the NaOH concentrations as discussed above. This can be explained by the fact that higher NaOH concentration can lead to the faster dissolution of the aluminosilicate phases, and thereby faster geopolymer formation (Ahmari et al., 2012; Rees et al., 2007), by which free As^V were consolidated and in turn stabilized (Liu et al., 2019; Opiso et al., 2021).

Furthermore, it is evident that extending the curing time from 7 to 28 days does not improve the compressive strength of these specimens too much (Fig. 3d) since specimens are likely to reach their ultimate compressive strength in 7 days for FA/MT-based geopolymer (Zhang et al., 2011). However, prolonging the curing time can significantly reduce the As^V leachabilities. For instance, in specimen with 54 wt% of FA, 0.03 wt% of As^V and activated with 10 M NaOH (i.e., FMA10G-02b), a reduction of As^V leachability from 1.33 mg L^{-1} to 0.01 mg L^{-1} was observed when extending the curing time from 7 to 28 days (Table 2). This is in good agreement with the previous report (Clancy et al., 2015), confirming that increased curing time appears to reduce the water permeability and porosity of the geopolymer, and thereby enhance the As^V S/S performance as expected.

Besides, the As^V immobilization efficiencies of all geopolymer specimens are above 95.4% (Fig. 3b), and As^V leachabilities of all specimens are below 5.0 mg L^{-1} as specified in the standard (Table 2). Moreover, the leachabilities of heavy metals of concern including copper (Cu), cadmium (Cd), lead (Pb), and chromium (Cr) are also below the MCLs (Table S2), indicating that all specimens comply with the Chinese leaching standard for hazardous wastes (GB 5085.3–2007) (PRC Ministry of Ecology and Environment, 2007). In addition, the leachability values of As^V and heavy metals of concern in geopolymers (i.e., the FMA10G-02 series) after curing for either 90 or 270 d are far below the MCLs as well (Table S3), endowing these materials with a long-term environmental safety. Therefore, the FA/MT-based geopolymers demonstrated superior immobilization performance for both As^V and typical heavy metals and high compressive strengths, particularly in specimens with 54 wt% of FA activated with 10 M NaOH (i.e., the FMA10G-02 series). Given their superior mechanical strengths and contaminant immobilization efficiency, FA/MT-based geopolymers can be used for remediation of As^V and heavy metal-contaminated sediments and the geopolymers with immobilized contaminants can be further used as low-carbon building materials.

3.5. *Immobilization mechanism of As^V*

To better understand the underlying mechanism responsible for As^V immobilization, several geopolymer specimens were collected and ground into fine powders for microstructural characterizations. XRD patterns of geopolymer specimens show evidence for calcium silicate (Ca_2SiO_4, JCPDS #31–0302), calcite ($CaCO_3$, JCPDS #05–0586), calcium silicate hydroxide (CSH, $Ca_5(SiO_4)_2(OH)_2$, JCPDS #29–0380), quartz (SiO_2, JCPDS #46–1045), and amorphous phases (Fig. 4, S5–7), all of which were commonly observed in fly ash-based geopolymers (Li et al., 2012; Rees et al., 2007). Of all specimens containing As^V, no evidence for crystalline calcium arsenate was identified, suggesting that precipitation with calcium ions seems not to be responsible for As^V immobilization. This is, however, contrary to preceding studies of stabilizing arsenic wastes at high levels with calcium-rich cementitious materials (Jiang et al., 2022; Wang et al., 2019) and is likely due to the low As^V loadings (i.e., 0.01–0.05 wt%) in this study.

Furthermore, it is worth to note that increasing the As^V contents

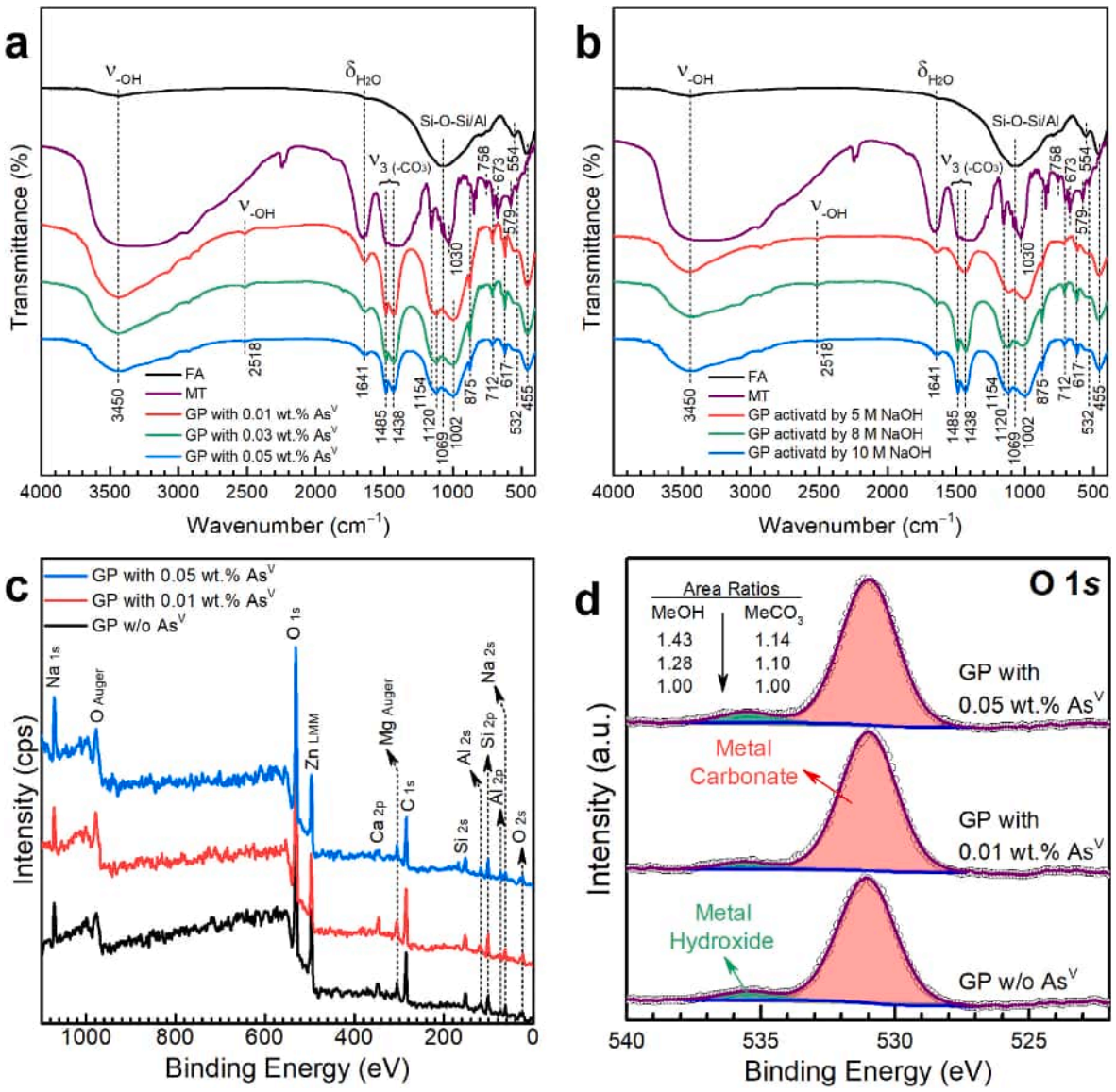

Fig. 6. FTIR spectra of (**a**) geopolymers (54 wt% FA, 10 M NaOH, 7-d curing) with varying As^V contents, (**b**) geopolymers (54 wt% FA, 0.05 wt% As^V, 7-d curing) activated with different concentrations of NaOH; XPS spectra of (**c**) survey scan, and (**d**) O 1s region on geopolymers (54 wt% FA, 10 M NaOH, 90-d curing) with varying As^V contents.

appears to enhance the phase transition from amorphous to crystalline (Fig. 4a and S5), with the highest crystallinity of the specimen containing the maximum As^V content (i.e., 0.05 wt%). This has also been observed in previous reports (Tian et al., 2021; Wang et al., 2019) and is likely owing to the hydration inhibition of geopolymer gel by arsenate. The NaOH concentration is also observed to have a profound effect on the phase composition of the geopolymer, and Fig. 4b and S6 illustrate the relationship between the NaOH concentration and the crystalline phase composition. There is an increase in the intensity of reflections at 2θ ~26.8° and 29.3° (attributed to calcium silicate and CSH, respectively) with increasing NaOH concentration, indicating that higher NaOH concentration accelerates the much more and faster formation of both calcium silicate and CSH, which is good agreement with the above discussion. Besides, CSH is believed to act as an effective encapsulator and physical barrier to prevent the leaching of toxic elements from the geopolymer (Bankowski et al., 2004; Opiso et al., 2021). This might explain why the specimens activated with 10 M NaOH demonstrated the best S/S performance towards As^V (Fig. 3 and Table 2). Of these specimens activated with 10 M NaOH, those with 54 wt% FA and 0.01 wt% As^V demonstrated a greater amount of amorphous geopolymer gels as compared to other specimens with different FA and As^V contents (Fig. 4a and c). Since the amorphous gel is likely to form a more compact geopolymer network than the specimens dominated by crystalline phases (Devi et al., 2020; Tian et al., 2021), and thereby leading to the maximum UCS (Fig. 2d) and the best S/S performance. As discussed earlier and expected, prolonging the curing time will eventually improve the development of crystalline phases (Fig. 4d, S7), resulting in loss of the compactness, and thus a slight decrease in the 28-day UCS values (Fig. 2d and the supplementary UCS data). It is of interest to note, however, that the specimens with 54 wt% and 10 M NaOH (i.e., the FMA10G-02 series) showed improved S/S performance towards As^V with increasing curing time (Fig. 3c–d, Table 2), regardless of the slight reduction in the 28-day UCS values (Fig. 2d). This observation reflects that As^V appears to be incorporated into the crystalline minerals (e.g., calcite, and CSHs) during the phase transition process over time (Li et al., 2019; Zhou et al., 2021).

SEM images of geopolymer specimens with 54 wt% FA are shown in Figs. 5 and 6, and S8. Obviously, three distinct particulates, i.e., the partially and unreacted FA particles, the unreacted MT, and the resultant geopolymer gels, can be identified. The unreacted FA particles are

Table 3
Assignment of characteristic vibrations to individual band in the geopolymer FTIR spectra.

Wavenumber (cm^{-1})	Characteristic vibrations	Reference
3550–3225, 3450	stretching (−OH)	(Ahmari et al., 2012; Ahmari and Zhang, 2012; Yu et al., 1999)
1798	$v_1 + v_4$ ($-CO_3$)	Sow (2016)
1641	bending (H–O–H)	(Li et al., 2019; Yu et al., 1999)
1485	asymmetric stretching (v_3, $-CO_3$)	(Sow, 2016; Tigue et al., 2018)
1438	asymmetric stretching (v_3, $-CO_3$)	(Li et al., 2019; Opiso et al., 2021; Sow, 2016)
950–1200	stretching (Si–O–Si, Si–O–Al)	(Ahmari et al., 2012; Lee and van Deventer, 2003; Rees et al., 2007; Yu et al., 1999)
1154	asymmetric stretching (Si–O–Si)	(Opiso et al., 2021; Rees et al., 2007)
1120	asymmetric stretching (Si–O–Si, Si–O–Al)	Lee and van Deventer (2003)
1069	asymmetric stretching (Si–O–Si, Si–O–Al), symmetric stretching (v_1, $-CO_3$)	(Lee and van Deventer, 2003; Opiso et al., 2021; Sow, 2016)
1030	asymmetric stretching (Si–O–Si, Si–O–Al), symmetric stretching (v_1, $-CO_3$)	(Rees et al., 2007; Sow, 2016; Tigue et al., 2018)
1002	symmetric stretching (v_1, $-CO_3$), Si–O in Q^2 sites	(Sow, 2016; Tigue et al., 2018)
875	out-of-plane bending (v_2, $-CO_3$)	(Ahmari et al., 2012; Jing et al., 2003; Sow, 2016)
758	bending (Si–O–Si, Si–O–Al)	(Opiso et al., 2021; Tigue et al., 2018)
712	in-plane bending (v_4, $-CO_3$)	(Jing et al., 2003; Li et al., 2019; Sow, 2016)
673	bending (Si–O–Si, in CSH)	(Yu et al., 1999; Zhang et al., 2019)
617	stretching (Si–O–Si, Si–O–Al)	Lee and van Deventer (2003)
579	bending (Si–O–Si, Si–O–Al)	Opiso et al. (2021)
554	bending (Si–O–Al)	(Lee and van Deventer, 2003; Opiso et al., 2021)
532	internal deformation of SiO_4	(Opiso et al., 2021; Yu et al., 1999)
455	bending (Si–O–Si)	Yu et al. (1999)

attached or surrounded by the gels which also consolidate and embed some partially reacted FA particles (Fig. 5, S8 and S9). No kidney bean-shaped particles corresponding to Gp can be found even in specimens with a Gp content of 5 wt% (Fig. S9), implying high reactivity of Gp particles in the geopolymerization reaction. It is worth noting that a large amount of unreacted FA particles remained in the geopolymer specimens (Fig. 5, S8 and S9), as compared to other FA/MT geopolymer (Zhang, N. et al., 2021). This is most likely due to the aggressive initial loss of water from the specimens during the heating process in oven, which probably inhibited the geopolymerization and thus resulted in a large amount of unreacted FA particles. Nevertheless, comparison of the micrographs in Fig. 5 indicates that as the NaOH concentration increased from 5 to 10 M, the number of unreacted FA particles decreased apparently and the specimens became more compact, implying a higher degree of geopolymerization at higher NaOH concentration (Ahmari et al., 2012; Zhang et al., 2011), which further confirms the above XRD results in Fig. 4. This observation provides direct microscopical evidence of the superior performance of specimens with 54 wt% FA and 10 M NaOH in both the compressive strength and the As^V immobilization (Figs. 2 and 3, and Table 2). Moreover, note that there is no significant change in the microstructure of the specimens with 54 wt% and 10 M NaOH after curing for 7 days (cf. Figs. S8b and c), confirming the UCS results that a large portion of the UCS was obtained within 7 days (Fig. 2d) (Zhang et al., 2011).

The FTIR spectra of geopolymer specimens with 54 wt% FA are shown in Fig. 6. The assignment of characteristic IR bands based on previous studies is summarized in Table 3. Apparently, neither vibrational band attributed to the symmetric stretching of As–O bond for the adsorbed As^V (i.e., ~830 cm^{-1}), nor bands associated with calcium arsenate (i.e., ~860 cm^{-1}) are identifiable in both IR spectra, suggesting that neither adsorption nor co-precipitation with calcium ions is likely to contribute to As^V immobilization (Jing et al., 2003). This is in good consistency with the above XRD results (Fig. 4). In general, the major Si–O–Si vibration band of the raw FA will undergo broadening and shifting toward a lower wavenumber after geopolymerization owing to the transition of ordered Si–O–Si structure to a less ordered structure with randomly distributed Si–O–Al bonds (Ahmari et al., 2012; Zhang et al., 2018). Comparison of the geopolymer IR spectra with that of FA reflects a clear shift of band at 1069 cm^{-1} (assignable to Si–O–Si/Al vibration) to a lower wavenumber at 1002 cm^{-1}, confirming the formation of geopolymer gels with a less ordered network as evidenced by the XRD data (Fig. 4). Besides, the intensity of the Si–O–Si/Al vibration bands near 1000 cm^{-1} decreased clearly with increasing As^V contents, indicating the reduction of the geopolymer gel amount as the As^V content increased. This is in good agreement with the above XRD results in Fig. 4a. It is worthy to note that the bands of asymmetric stretching vibration (v_3, $-CO_3$) in surface $CaCO_3$ at 1438 and 1485 cm^{-1} weaken as well with increasing As^V contents (Fig. 6a). This observation can be explained by the fact that the specimen with the least As^V content (i.e., FMA10G-02a) holds the maximum amorphous phases (Fig. 4a), which are more reactive than the crystalline phases in specimens with higher As^V content (i.e., FMA10G-02b, and FMA10G-02c, see Fig. 4a) to react with CO_2 in the air to form the surface $CaCO_3$.

The XPS spectra of geopolymers (54 wt% FA, 10 M NaOH, 90-d curing) with varying As^V contents are given in Fig. 6c and d, and S10. It is of interest to note that no peaks attributable to As^V were observed even for specimen with 0.05 wt% of As^V (Fig. 6c), and that the peak areas of O 1*s* region (assignable to metal carbonate and hydroxide, respectively) grew with As^V contents (Fig. 6d), confirming the above speculation that As^V appears to be incorporated into the calcite and CSHs-related crystals upon the long-term curing. The XPS spectra of C 1*s*, Si 2*p*, Al 2*p*, and Ca 2*p* regions (Fig. S10) revealed that these metals are in the form of carbonates or CSHs-related hydroxides, which can be further verified by the XRD patterns (Fig. S11). Given the above analyses, we believe that As^V appears to be encapsulated in geopolymer gels after curing for a very short period, and then incorporated into the crystalline minerals (e.g., calcite, calcium silicate and CSHs) during the phase transition processes as a result of long-term curing (i.e., 28 days and beyond) (Li et al., 2019; Zhou et al., 2021).

4. Conclusion

In this study, we have developed FA/MT-based geopolymers and evaluated the practicability of immobilizing exogenetic As^V in geopolymer matrices. The results of compressive strength tests showed that all variables including FA content, As^V content, NaOH concentration, and curing time can affect the strength development of geopolymers, and that the optimal formulation demonstrating the maximum compressive strength (i.e., 37.07 MPa) attributes to the specimen containing 54 wt% FA, 0.03 wt% As^V activated with 10 M NaOH and cured for 28 days. Surprisingly, our TCLP leaching test results of either As^V or other heavy metals of concern revealed that both the short-term and long-term leachabilities of all toxics in geopolymers with varying compositions are below the standard MCLs even at exogenetic As^V addition up to 0.05 wt%, in spite of the fact that the leachability of Pb in MT exceeded the MCL value by 3.3 times. Microstructural characterization data implied that calcite, calcium silicate, and calcium silicate hydroxide (CSH) are likely to play a crucial role in immobilizing As^V and heavy metals of concern in the resultant matrixes. The FA/MT-based geopolymers can be potentially used as low-carbon S/S materials for arsenic-contaminated soil remediation and as building materials given their superior mechanical strengths and long-term stabilities.

Authorship contribution statement

Alseny Bah: Methodology, Visualization, Investigation, Writing – original draft.

Jie Jin: Methodology, Visualization, Investigation.

Andrea O. Ramos: Methodology, Visualization, Investigation.

Yang Bao: Methodology, Investigation.

Mengyu Ma: Methodology, Investigation.

Feihu Li: Conceptualization, Visualization, Methodology, Writing – review & editing, Funding acquisition, Supervision.

Declaration of competing interest

The authors declare that they have no known competing financial interests or personal relationships that could have appeared to influence the work reported in this paper.

Data availability

Data will be made available on request.

Acknowledgments

The work was partially supported by the National Natural Science Foundation of China (51002080, 51310105009). We are grateful to Dr. Fengying Li for providing the portable XRF apparatus. We thank the anonymous reviewers for their constructive comments.

Appendix A. Supplementary data

Supplementary data to this article can be found online at https://doi.org/10.1016/j.chemosphere.2022.135636.

References

Ahmari, S., Ren, X., Toufigh, V., Zhang, L.Y., 2012. Production of geopolymeric binder from blended waste concrete powder and fly ash. Construct. Build. Mater. 35, 718–729. https://doi.org/10.1016/j.conbuildmat.2012.04.044.

Ahmari, S., Zhang, L.Y., 2012. Production of eco-friendly bricks from copper mine tailings through geopolymerization. Construct. Build. Mater. 29, 323–331. https://doi.org/10.1016/j.conbuildmat.2011.10.048.

Akhter, H., Cartledge, F.K., Roy, A., Tittlebaum, M.E., 1997. Solidification/stabilization of arsenic salts: effects of long cure times. J. Hazard Mater. 52 (2–3), 247–264. https://doi.org/10.1016/S0304-3894(96)01811-0.

Alka, S., Shahir, S., Ibrahim, N., Ndejiko, M.J., Vo, D.V.N., Abd Manan, F., 2021. Arsenic removal technologies and future trends: a mini review. J. Clean. Prod. 278, 123805 https://doi.org/10.1016/j.jclepro.2020.123805.

Allahverdi, A., Kani, E.N., 2009. Construction wastes as raw materials for geopolymer binders. Int. J. Civ. Eng. 7 (3), 154–160.

Bah, A., Feng, D.L., Kedjanyi, E.A.K., Shen, Z.Y., Bah, A., Li, F.H., 2022. Solidification of (Pb-Zn) mine tailings by fly ash-based geopolymer I: influence of alkali reagents ratio and curing condition on compressive strength. J. Mater. Cycles Waste Manag. 24 (1), 351–363. https://doi.org/10.1007/s10163-021-01322-4.

Bankowski, P., Zou, L., Hodges, R., 2004. Using inorganic polymer to reduce leach rates of metals from brown coal fly ash. Miner. Eng. 17 (2), 159–166. https://doi.org/10.1016/j.mineng.2003.10.024.

Capasso, I., Lirer, S., Flora, A., Ferone, C., Cioffi, R., Caputo, D., Liguori, B., 2019. Reuse of mining waste as aggregates in fly ash-based geopolymers. J. Clean. Prod. 220, 65–73. https://doi.org/10.1016/j.jclepro.2019.02.164.

Choi, W.H., Lee, S.R., Park, J.Y., 2009. Cement based solidification/stabilization of arsenic-contaminated mine tailings. Waste Manage. (Tucson, Ariz.) 29 (5), 1766–1771. https://doi.org/10.1016/j.wasman.2008.11.008.

Clancy, T.M., Snyder, K.V., Reddy, R., Lanzirotti, A., Amrose, S.E., Raskin, L., Hayes, K. F., 2015. Evaluating the cement stabilization of arsenic-bearing iron wastes from drinking water treatment. J. Hazard Mater. 300, 522–529. https://doi.org/10.1016/j.jhazmat.2015.07.051.

Devi, P., Kothari, P., Dalai, A.K., 2020. Stabilization and solidification of arsenic and iron contaminated canola meal biochar using chemically modified phosphate binders. J. Hazard Mater. 385, 121559 https://doi.org/10.1016/j.jhazmat.2019.121559.

Diaz-Loya, E.I., Allouche, E.N., Eklund, S., Joshi, A.R., Kupwade-Patil, K., 2012. Toxicity mitigation and solidification of municipal solid waste incinerator fly ash using alkaline activated coal ash. Waste Manage. (Tucson, Ariz.) 32 (8), 1521–1527. https://doi.org/10.1016/j.wasman.2012.03.030.

Giels, M., Iacobescu, R.I., Cappuyns, V., Pontikes, Y., Elsen, J., 2019. Understanding the leaching behavior of inorganic polymers made of iron rich slags. J. Clean. Prod. 238, 117736 https://doi.org/10.1016/j.jclepro.2019.117736.

Izquierdo, M., Querol, X., Davidovits, J., Antenucci, D., Nugteren, H., Fernandez-Pereira, C., 2009. Coal fly ash-slag-based geopolymers: microstructure and metal leaching. J. Hazard Mater. 166 (1), 561–566. https://doi.org/10.1016/j.jhazmat.2008.11.063.

Jiang, G.H., Min, X.B., Ke, Y., Liang, Y.J., Yan, X., Xu, W.B., Lin, Z., 2022. Solidification/stabilization of highly toxic arsenic-alkali residue by MSWI fly ash-based cementitious material containing Friedel's salt: efficiency and mechanism. J. Hazard Mater. 425, 127992 https://doi.org/10.1016/j.jhazmat.2021.127992.

Jing, C.Y., Korfiatis, G.P., Meng, X.G., 2003. Immobilization mechanisms of arsenate in iron hydroxide sludge stabilized with cement. Environ. Sci. Technol. 37 (21), 5050–5056. https://doi.org/10.1021/es021027g.

Kavitha, O.R., Shanthi, V.M., Arulraj, G.P., Sivakumar, V.R., 2016. Microstructural studies on eco-friendly and durable Self-compacting concrete blended with metakaolin. Appl. Clay Sci. 124, 143–149. https://doi.org/10.1016/j.clay.2016.02.011.

Lee, W.K.W., van Deventer, J.S.J., 2003. Use of infrared spectroscopy to study geopolymerization of heterogeneous amorphous aluminosificates. Langmuir 19 (21), 8726–8734. https://doi.org/10.1021/la026127e.

Li, Q., Xu, H., Li, F.H., Li, P.M., Shen, L.F., Zhai, J.P., 2012. Synthesis of geopolymer composites from blends of CFBC fly and bottom ashes. Fuel 97, 366–372. https://doi.org/10.1016/j.fuel.2012.02.059.

Li, Y.C., Min, X.B., Chai, L.Y., Shi, M.Q., Tang, C.J., Wang, Q.W., Liang, Y.J., Lei, J., Liyang, W.J., 2016. Co-treatment of gypsum sludge and Pb/Zn smelting slag for the solidification of sludge containing arsenic and heavy metals. J. Environ. Manag. 181, 756–761. https://doi.org/10.1016/j.jenvman.2016.07.031.

Li, Y.C., Min, X.B., Ke, Y., Fei, J.C., Liu, D.G., Tang, C.J., 2019. Immobilization potential and immobilization mechanism of arsenic in cemented paste backfill. Miner. Eng. 138, 101–107. https://doi.org/10.1016/j.mineng.2019.04.041.

Liu, D.G., Ke, Y., Min, X.B., Liang, Y.J., Wang, Z.B., Li, Y.C., Fei, J.C., Yao, L.W., Xu, H., Jiang, G.H., 2019. Cotreatment of MSWI fly ash and granulated lead smelting slag using a geopolymer system. Int. J. Environ. Res. Publ. Health 16 (1), 156. https://doi.org/10.3390/ijerph16010156.

Nidheesh, P.V., Singh, T.S.A., 2017. Arsenic removal by electrocoagulation process: recent trends and removal mechanism. Chemosphere 181, 418–432. https://doi.org/10.1016/j.chemosphere.2017.04.082.

Opiso, E.M., Tabelin, C.B., Maestre, C.V., Aseniero, J.P.J., Park, I., Villacorte-Tabelin, M., 2021. Synthesis and characterization of coal fly ash and palm oil fuel ash modified artisanal and small-scale gold mine (ASGM) tailings based geopolymer using sugar mill lime sludge as Ca-based activator. Heliyon 7 (4), e06654. https://doi.org/10.1016/j.heliyon.2021.e06654.

Palansooriya, K.N., Shaheen, S.M., Chen, S.S., Tsang, D.C.W., Hashimoto, Y., Hou, D.Y., Bolan, N.S., Rinklebe, J., Ok, Y.S., 2020. Soil amendments for immobilization of potentially toxic elements in contaminated soils: a critical review. Environ. Int. 134, 105046 https://doi.org/10.1016/j.envint.2019.105046.

Podgorski, J., Berg, M., 2020. Global threat of arsenic in groundwater. Science 368 (6493), 845–850. https://doi.org/10.1126/science.aba1510.

PRC Ministry of Ecology and Environment, 2007. Identification Standards for Hazardous Wastes (GB 5085.3 - 2007). Beijing, China.

Rees, C.A., Provis, J.L., Lukey, G.C., van Deventer, J.S.J., 2007. In situ ATR-FTIR study of the early stages of fly ash geopolymer gel formation. Langmuir 23 (17), 9076–9082. https://doi.org/10.1021/la701185g.

Rovnanik, P., 2010. Effect of curing temperature on the development of hard structure of metakaolin-based geopolymer. Construct. Build. Mater. 24 (7), 1176–1183. https://doi.org/10.1016/j.conbuildmat.2009.12.023.

Rowles, M., O'Connor, B., 2003. Chemical optimisation of the compressive strength of aluminosilicate geopolymers synthesised by sodium silicate activation of metakaolinite. J. Mater. Chem. 13 (5), 1161–1165. https://doi.org/10.1039/b212629j.

Shan, C.C., Jing, Z.Z., Pu, L., Pan, X.H., 2012. Solidification of MSWI ash at low temperature of 100 degrees C. Ind. Eng. Chem. Res. 51 (28), 9540–9545. https://doi.org/10.1021/ie203040d.

Shi, C.J., Qu, B., Provis, J.L., 2019. Recent progress in low-carbon binders. Cement Concr. Res. 122, 227–250. https://doi.org/10.1016/j.cemconres.2019.05.009.

Singh, R., Singh, S., Parihar, P., Singh, V.P., Prasad, S.M., 2015. Arsenic contamination, consequences and remediation techniques: a review. Ecotoxicol. Environ. Saf. 112, 247–270. https://doi.org/10.1016/j.ecoenv.2014.10.009.

Singh, T.S., Pant, K.K., 2006. Solidification/stabilization of arsenic containing solid wastes using portland cement, fly ash and polymeric materials. J. Hazard Mater. 131 (1–3), 29–36. https://doi.org/10.1016/j.jhazmat.2005.06.046.

Sow, P.Y., 2016. IR-spectroscopic Investigations of the Kinetics of Calcium Carbonate Precipitation. University of Konstanz, Konstanz, Germany.

Tian, Q.Z., Chen, C.S., Wang, M.M., Guo, B.L., Zhang, H.J., Sasaki, K., 2021. Effect of Si/Al molar ratio on the immobilization of selenium and arsenic oxyanions in geopolymer. Environ. Pollut. 274, 116509 https://doi.org/10.1016/j.envpol.2021.116509.

Tigue, A.A.S., Malenab, R.A.J., Dungca, J.R., Yu, D.E.C., Promentilla, M.A.B., 2018. Chemical stability and leaching behavior of one-Part Geopolymer from soil and coal fly ash mixtures. Minerals 8 (9), 411. https://doi.org/10.3390/min8090411.

U.S. Environmental Protection Agency, 1992. Method 1311: Toxicity Characteristic Leaching Procedure. Washington, DC.

van Jaarsveld, J.G.S., van Deventer, J.S.J., Lukey, G.C., 2002. The effect of composition and temperature on the properties of fly ash- and kaolinite-based geopolymers. Chem. Eng. J. 89 (1–3), 63–73. https://doi.org/10.1016/S1385-8947(02)00025-6.

Wang, L., Chen, L., Guo, B.L., Tsang, D.C.W., Huang, L.B., Ok, Y.S., Mechtcherine, V., 2020. Red mud-enhanced magnesium phosphate cement for remediation of Pb and as contaminated soil. J. Hazard Mater. 400, 123317 https://doi.org/10.1016/j.jhazmat.2020.123317.

Wang, L., Cho, D.W., Tsang, D.C.W., Cao, X.D., Hou, D.Y., Shen, Z.T., Alessi, D.S., Ok, Y.S., Poon, C.S., 2019. Green remediation of as and Pb contaminated soil using cement-free clay-based stabilization/solidification. Environ. Int. 126, 336–345. https://doi.org/10.1016/j.envint.2019.02.057.

Yu, P., Kirkpatrick, R.J., Poe, B., McMillan, P.F., Cong, X.D., 1999. Structure of calcium silicate hydrate (C-S-H): near-, mid-, and far-infrared spectroscopy. J. Am. Ceram. Soc. 82 (3), 742–748. https://doi.org/10.1111/j.1151-2916.1999.tb01826.x.

Zhang, L.Y., Ahmari, S., Zhang, J.H., 2011. Synthesis and characterization of fly ash modified mine tailings-based geopolymers. Construct. Build. Mater. 25 (9), 3773–3781. https://doi.org/10.1016/j.conbuildmat.2011.04.005.

Zhang, N., Hedayat, A., Sosa, H.G.B., Bernal, R.P.H., Tupa, N., Morales, I.Y., Loza, R.S.C., 2021. On the incorporation of class F fly-ash to enhance the geopolymerization effects and splitting tensile strength of the gold mine tailings-based geopolymer. Construct. Build. Mater. 308, 125112 https://doi.org/10.1016/j.conbuildmat.2021.125112.

Zhang, W., Yao, X., Yang, T., Liu, C., Zhang, Z.H., 2018. Increasing mechanical strength and acid resistance of geopolymers by incorporating different siliceous materials. Construct. Build. Mater. 175, 411–421. https://doi.org/10.1016/j.conbuildmat.2018.03.195.

Zhang, X.L., Zhang, S.Y., Hui, L., Zhao, Y.L., 2021. Disposal of mine tailings via geopolymerization. J. Clean. Prod. 284, 124756 https://doi.org/10.1016/j.jclepro.2020.124756.

Zhang, Y.Y., Zhang, S.Q., Ni, W., Yan, Q.H., Gao, W., Li, Y.Y., 2019. Immobilisation of high-arsenic-containing tailings by using metallurgical slag-cementing materials. Chemosphere 223, 117–123. https://doi.org/10.1016/j.chemosphere.2019.02.030.

Zhou, X., Zhang, Z.F., Yang, H., Bao, C.J., Wang, J.S., Sun, Y.H., Liu, D.W., Shen, P.L., Su, C., 2021. Red mud-metakaolin based cementitious material for remediation of arsenic pollution: stabilization mechanism and leaching behavior of arsenic in lollingite. J. Environ. Manag. 300, 113715 https://doi.org/10.1016/j.jenvman.2021.113715.